

Wavelet-Based Statistical Analysis versus SPM of Brain Imaging Data

Radu Mutihac*

University of Bucharest, Department of Electricity and Biophysics, ROMANIA

Received 8 February 2007; Revised 28 February 2008; Accepted 8 April 2008

Abstract

Analysis of functional magnetic resonance imaging (fMRI) data of a block-based visual stimulation paradigm was comparatively performed by the discrete wavelet transform (DWT) in the wavelet domain and statistical parametric mapping (SPM) within the framework of the general linear model (GLM) [1]. The link is supported by the low-pass analysis filter of the DWT that can be similarly shaped to a Gaussian filter in SPM and by the subsampling scheme that provides means to define the number of coefficients in the low-pass subband of the wavelet decomposition [2]. Functional data processing in the wavelet domain was carried out by means of two biorthogonal transforms resulting in activation patterns similar to the activation maps obtained in SPM.

Keywords

Wavelets, Multiresolution Analysis, Functional Magnetic Resonance Imaging, General Linear Model, Statistical Parametric Mapping

1. INTRODUCTION

Analysis of fMRI data, the most complex biomedical time series, is a non-invasive method that allows localization in time and space of the dynamic processes of the intact living brain. The widely spread index of neuronal activity is the blood oxygenation level dependent (BOLD) contrast [3], which is based on the differing magnetic susceptibilities of oxygenated hemoglobin (diamagnetic) and deoxygenated hemoglobin (paramagnetic) in relation with the surrounding tissue. The central assumption is that an increase in neuronal activity within a brain region leads to hyperoxemia, which attracts an increase in local blood flow and reduced concentrations of deoxyhemoglobin in the blood vessels. Changes in blood flow, which are closely coupled to functional activation, indicate brain areas involved in various tasks that subjects perform in the scanner. These changes and oxygenation variability (vascular and hemodynamic) are temporally delayed relative to the neural firing with the hemodynamic lag.

The BOLD methods are sensitive to artifacts associated with head and/or vessel motion, vascular inflow, and drainage effects. Quite often, the artifacts are correlated with the signal of interest and, therefore, not discarded by simple image averaging. Still BOLD-based neuroimaging methods are generally superior to any imaging modality in terms of: (i) equipment availability, (ii) no need of exogenous contrast agents or exposing to ionizing radiation, (iii) best spatial resolution, and (iv) activation images can be coregistered with anatomical images acquired on the same machine [4].

The main task in statistical analysis of functional brain imaging data is to come out with a summarizing map of a statistic that specifies the locations of activity elicited by the experimental paradigm. These areas are routinely identified by setting an appropriate threshold and retaining as significant those anatomical locations where the statistical field is higher than the chosen level. The threshold is usually computed following criteria derived from the Gaussian Random Field Theory

* Corresponding author information: Radu Mutihac, University of Bucharest, Faculty of Physics, Department of Electricity and Biophysics, PO Box MG-11, Bucharest 077125 Romania, Phone: (4072)702-0772; Fax: (4021)315-9249; E-mail: mutihac@gmail.com.

(RFT). This approach provides the probability of false positives for a certain threshold given a statistical field of some smoothness. The higher the smoothness, the higher is the correlation among adjacent locations, the lower the risk of a noise field crossing the selected threshold. However, by smoothing the field with a filter of fixed resolution, the probability of detecting signals of that particular size is maximized, yet sharper foci might be wiped off and/or signals of varying spatial scale could erroneously be detected.

The latter drawback is overcome by multiresolution analysis (MRA) that employs a number of different smoothing levels and sets the threshold accordingly. Thresholding the statistical fields equates to “modeling” the noise rather than the signal, since it comes out with a binary output: everything over the threshold is unlikely to be noise, everything under the threshold is likely to be noise [5]. As such, the activation areas can be detected, yet the shape, scale, and intensity of signals remain unknown since the suprathresholded statistic values are still subject to noise. Wavelet methods approach the analysis of statistical fields by estimating the signal at any resolution among the random fluctuations and providing some degree of localization in space and frequency as well. Since the interest in fMRI data is focused on relatively spatially localized signals, wavelets are appropriate to represent them by a small number of strong local coefficients, whereas the power of white noise is uniformly spread throughout the wavelet space.

A *wavelet transform* (WT) amounts to the representation of a function (e.g., signal) by wavelets. Wavelet *shrinkage* refers to reconstructions obtained by means of some WT of the original signal, followed by shrinking the wavelet coefficients towards zero, and back transforming of the remained wavelet coefficients by the inverse WT (IWT) onto the signal space [6]. Wavelet-based shrinkage methods are nonparametric regression estimators that provide means of finding structure in a variety of data sets

without imposing a parametric regression model.

The WTs are becoming increasingly spread in different areas of applied and theoretical science. By truncating the wavelet coefficients below a certain threshold, data become sparsely represented, which renders wavelets suitable for data compression and quite similar to the topographic independent component analysis (ICA) [7,8]. Here, the point is that the structured component of a signal is well represented by a relatively few wavelet coefficients, whereas its unstructured components like noise project quasi-equally onto all basis functions. Consequently, the structured and unstructured parts of the signal come out separated in the WT domain. As such, wavelets outperform Fourier representations in accurately deconstructing and reconstructing finite, non-periodic and/or non-stationary signals such as functional neuroimaging data.

The continuous WT (CWT) is commonly applied in Physics, whereas the discrete WT (DWT) is more common in numerical analysis, signal, and image processing. The main tasks of wavelets in imaging are compression and denoising of images, as well as image/contrast enhancement.

2. METHODS

Wavelets appeared as the consequence of the interest shifting from *frequency analysis* to *scale analysis*, which entailed the design of mathematical structures that vary in scale. In approximation using superposition of functions, Fourier basis functions (sines and cosines) are non-local and stretch out to infinity, rendering them unsuited to analyze rapidly varying signals [9]. In contrast, wavelets are mathematical functions developed to analyze data at different *scales* or *resolutions*. The interest in wavelets is also due to computationally efficient implementation in MRA. Just as fast Fourier transform (FFT) algorithms made the Fourier Transform (FT) a practical tool for spectral analysis, the MRA has made the DWT a viable tool for computational time-scale analysis.

Wavelet and Scaling Functions

Both for practical and theoretical reasons, wavelets are chosen as continuously differentiable functions with compact support from a subspace of the space $L_1(\mathbb{R}) \cap L_2(\mathbb{R})$, which is the space of measurable functions that are absolutely and square integrable (e.g., finite energy) in the Lebesgue's sense:

$$\int_{-\infty}^{+\infty} |f(x)| dx < +\infty \quad \text{and} \quad \int_{-\infty}^{+\infty} |f(x)|^2 dx < +\infty \quad (1)$$

Recall that, if $p \in \mathbb{R}$, $p \geq 1$ and (S, μ) is a measure space, then the $L_p(S, \mu)$ is a Banach space abbreviated $L_p(\mu)$, or just L_p , consisting of all measurable functions from S to \mathbb{C} (or \mathbb{R}) [10] such as:

$$\|f(x)\|_{L_p} \triangleq \int_{-\infty}^{+\infty} (|f(x)|^p)^{\frac{1}{p}} d\mu < +\infty \quad (2)$$

Wavelet analysis procedure is to adopt some two continuously-defined functions:

1. The *scaling function* (or *father function*) $\phi(x)$ is the solution of a *two-scale equation*:

$$\phi(x) = \sqrt{2} \sum_{k \in \mathbb{Z}} h(k) \phi(2x - k) \quad (3)$$

where the sequence $\{h(k)\}_{k \in \mathbb{Z}}$ is the *refinement filter*.

2. Its associated *wavelet function* $\psi(x)$, alternatively called *prototype* or *mother wavelet function*:

$$\psi(x) = \sqrt{2} \sum_{k \in \mathbb{Z}} g(k) \phi(2x - k) \quad (4)$$

where $\{g(k)\}_{k \in \mathbb{Z}}$ is a suitable weighting sequence.

As such, one may enforce the conditions of zero mean:

$$\int_{-\infty}^{+\infty} \psi(x) dx = 0 \quad (5)$$

and square norm one:

$$\int_{-\infty}^{+\infty} |\psi(x)|^2 dx = 1 \quad (6)$$

Wavelets are the building blocks of the WTs the same way that sines and cosines are the building blocks of the Fourier transform (FT). Yet wavelets (almost) can be supported on an arbitrarily small closed interval, which makes wavelets a suitable tool in handling phenomena that change rapidly in time. Details at various levels of resolution are represented by the superposition of wavelets associated with the appropriate dilations. Complex data can be inspected by dilation, which performs “zoom-in” on details. Reversely, details can be suppressed by stretching, which behaves like “zoom-out”; therefore, wavelets are appropriate candidates for data smoothing.

Wavelet Basis Functions

Brain signals are complex, quite unknown, and difficult to model, so that optimal basis functions cannot be specified in advance. Wavelet MRA alleviates this difficulty by detecting and extracting the underlying signal features over many scales. The continuous-time interpretation of the wavelet decomposition is based on the fundamental concept of *scaling* or *scale-varying* function. Scale-varying basis functions render signal processing less sensitive to noise because of measuring the average fluctuations of a signal at different scales.

Wavelet construction starts from the basic mother wavelet, $\psi(x)$, which generates the basis by *dilation* (index j) and *translation* (index k) in time $\psi(ax - b)$. For the discrete wavelets, the parameter of translation, b , and dilation, a , are restricted to discrete sets, usually $a = 2^j$ and $b = k$, where $j, k \in \mathbb{Z}$. Dilation allows hierarchical representation of a data set. *Temporal* analysis is performed with a contracted, high-frequency version of the prototype wavelet, while *frequency* analysis is performed with a dilated, low-frequency version of the same wavelet:

$$\psi_{j,k} = 2^{-j/2} \psi(x/2^{-j} - k) \quad (5)$$

The collection of shifted and scaled wavelet functions forms a *wavelet basis*. Most often, the grid in shift-scale space on which the wavelet basis functions are defined is *dyadic*. Any continuous function (e.g., signal or image) is uniquely projected onto the wavelet basis functions and expressed as a *linear combination* of the basis functions. The set of coefficients which weight the wavelet basis functions in such representation is referred to as the *wavelet transform* (WT) of the given function. A *discrete wavelet transform* is any WT for which the wavelets are discretely sampled. In a *continuous wavelet transform*, a signal of finite energy is projected on a continuous family of frequency bands or similar subspaces of $L_2(\mathbb{R})$. Both the DWT and CWT are analog transforms developed to represent continuous-time (analog) signals. The CWTs operate over any admissible scale and translation, whereas the DWTs employ a specific subset of scale and translation values or representation grid.

Orthogonal basis functions

The *orthogonality* property means that the inner product of the mother wavelet with itself is unity, and the inner products between the mother wavelet and the aforementioned shifts and dilates of the mother wavelet are zero. Orthogonal wavelet basis functions can be found by appropriate choice of the sequences $\{h(k)\}_{k \in \mathbb{Z}}$ and $\{g(k)\}_{k \in \mathbb{Z}}$ or, equivalently, setting appropriate functions, φ and ψ , such that $\{\psi_{j,k}\}_{j,k \in \mathbb{Z}}$ forms an orthonormal basis of $L_2(\mathbb{R})$, that is:

$$\langle \tilde{\psi}_{j,k}, \psi_{i,l} \rangle = \delta_{j-i} \cdot \delta_{k-l}, \quad i, j, k, l \in \mathbb{Z} \quad (6)$$

where $\{\tilde{\psi}_{j,k}\}_{j,k \in \mathbb{Z}}$ are the *biorthogonal basis functions* of $\{\psi_{j,k}\}_{j,k \in \mathbb{Z}}$. Hence, any function $f(x) \in L_2$ can be uniquely represented by the expansion:

$$f(x) = \sum_{j \in \mathbb{Z}} \sum_{k \in \mathbb{Z}} d_j(k) \psi_{j,k}(x) + \sum_{j \in \mathbb{Z}} \sum_{k \in \mathbb{Z}} a_j(k) \phi_{j,k}(x) \quad (7)$$

where the detail coefficients $\{d_j(k)\}_{j,k \in \mathbb{Z}}$ and the approximation coefficients $\{a_j(k)\}_{j,k \in \mathbb{Z}}$, due to orthogonality, are obtained by forming the inner products of the function $f(x) \in L_2$ with the corresponding basis functions:

$$d_j(k) = \langle f, \psi_{j,k} \rangle_{L_2}, \quad a_j(k) = \langle f, \phi_{j,k} \rangle_{L_2}, \quad j, k \in \mathbb{Z} \quad (8)$$

The decomposition of any function $f(x) \in L_2$ is practically carried out on a finite number of scales only, say J , resulting in:

$$f(x) = \sum_{j=1}^J \sum_{k \in \mathbb{Z}} d_j(k) \psi_{j,k}(x) + \sum_{k \in \mathbb{Z}} c_J(k) \phi_{J,k} \quad (9)$$

The wavelet coefficients are efficiently calculated using Mallat's algorithm [11], which is based on a hierarchical application of the filterbank decomposition.

The wavelet-space partitions exhibiting improved localized SNR conditions can be exploited by orthogonal wavelet decomposition. Since data can be represented in terms of wavelet expansion, any operation on data can be carried out using the corresponding wavelet coefficients only. Then the statistical analysis can be restricted for the significant coefficients to these partitions only. The potential benefits are improved SNR and a decrease of the detection threshold due to the reduced number of statistical tests, both contributing to a higher detection sensitivity with no increase in type I errors (false positives) [4].

Wavelet Families

Wavelet families and functions provide a rich space in which to search for a wavelet which optimally represents any function of interest. Any WT yields an efficient representation for functions which have similar characters to the functions in the wavelet basis. Unlike the case

of the FT, a large selection of wavelet families is available depending on the mother wavelet. Some desirable properties like orthogonality, compactness of support, rapid decay, and smoothness impose several restrictions on the choice of the mother wavelet. Various wavelet families are a trade-off between their spatial compactness and smoothness.

Orthogonal spline wavelets are recommended in neuroimaging data analysis for a number of reasons: (i) *orthogonality* is required by the subsequent statistical analysis; (ii) the resulting family of transforms use *symmetric basis functions*; (iii) the usage of splines reduces spectral overlap between resolution channels by increasing the degree of spline n [4,12]. Nevertheless, small spectral overlap increases data decorrelation [13], which raises the detection sensitivity. The decorrelation ability of orthogonal spline wavelets stems from the fact that splines with degree n yield $n+1$ vanishing moments. The uncertainty principle limits the level of decorrelation across scale since the correlation suppression comes at the expense of a loss in spatial localization expressed in the decay rate of the filter coefficients. Besides, selecting the degree of splines depends to some extent on the assumed smoothness of the signal to be detected. Smooth wavelet bases are asymptotically near-optimal for estimating signals that may contain some points of discontinuity [14]. The orthonormal, smooth wavelet basis functions, albeit symmetric, cannot have compact support but exhibit exponential decay [15]. Moreover, symmetric cubic spline orthonormal basis functions do not introduce phase distortions, hence a better localization of the signal in the WT domain.

Functional Brain Imaging Analysis

The goal in neuroimaging data analysis is to maximally suppress noise along with preserving as much as possible of the image features. In a wavelet representation, the wavelet coefficients carry both time and frequency information, as the basis functions vary in position and scale. In contrast to spatial filtering with a Gaussian kernel, wavelet

shrinkage allows locally adaptive bandwidth so that the power to detect spatial features of varying extent is not constrained by the arbitrary choice of a single kernel size [16]. As such, the preprocessed fMRI data are subject to spatial non-redundant DWT, rather than spatially convolved with a Gaussian kernel.

It is a common practice in MRI to use magnitude images in order to alleviate the problem of phase artifacts by deliberately discarding the phase information. The raw signal is measured by a quadrature detector, which yields the real and the imaginary raw data. The complex FT is employed to reconstruct the real and the imaginary images from the acquired data. The SNR in the real and imaginary images is primarily affected by the resistance of the receiving RF coil and the inductive losses in the sample [17]. Assuming each channel contaminated with white noise, the FT enforces preservation of the Gaussian character of the noise distribution in the real and imaginary images, and uncorrelated noise between the corresponding real and imaginary voxels due to the uniform variance of the noise over the whole field of view. Next, the magnitude images are obtained from the real and imaginary images by calculating the modulus pixel-by-pixel. This mapping is a nonlinear process, so that the noise in the magnitude image is no longer Gaussian [18]. Noise in the final image is supplementary influenced by the voxel size, the receiver bandwidth, and the number of averages (if any) during image acquisition [19]. Most of the standard statistical tests in fMRI assume Gaussian distributed noise, though MR magnitude image data was found to obey a Rician distribution [18-20]. Unlike the additive Gaussian noise, the Rician noise is multiplicative (i.e., signal-dependent), which makes difficult to separate the noise from the signal. The Rician noise is especially problematic in low SNR regimes like $\text{SNR} < 2$, where it causes random fluctuations and introduces a signal-dependent bias to data that reduces the image contrast [21]. The noise distribution is nearly Gaussian for $\text{SNR} > 2$ [18]. Therefore, wavelet-based noise removal

methods that adapt to variations of both signal and noise are attractive for filtering out the Rician noise.

The BOLD contrast is nevertheless analyzed as the difference between two MR images (e.g., activation minus baseline) both containing Rician distributed noise; the distribution of noise appears symmetric and closely approximates a Gaussian curve. Moreover, for very low signal intensities, a deviation from Gaussianity was evaluated on the basis of Kolmogorov-Smirnoff (KS) test and found statistically significant in very large images only [22].

We applied a method proposed by Donoho and Johnstone [23] to find the threshold that minimizes the estimate of the mean squared error (MSE). The approach equates to applying a soft thresholding nonlinearity, with the threshold selected by the Stein's unbiased risk estimate (SURE) in the $[0, \sqrt{2 \log n}]$, where

$n = 2^J$ is the data number and J is the number of scales. This was proved to possess various optimality properties for MSE estimation. The SURE shrinkage performs the best reconstruction of signals both in terms of noise suppression and sharp structure preservation in the neighborhood of the highly-variable spatial components.

3. RESULTS AND DISCUSSION

The main interest in functional neuroimaging studies lays in the electrical activity of firing neurons, which cannot be directly investigated by MRI or be entirely inferred by analyzing the vascular process either. The reasons are: (i) the hemodynamic lag varies in a complex way from tissue to tissue, and (ii) no theory on the relationship between the electrical and hemodynamic processes is available to date. Yet the vascular process provides valuable information for the electrical activity in firing neurons that advocates for the interest in fMRI data analysis.

Data Acquisition and Preprocessing

One healthy subject was selected for single-shot MR FEEPI scanning at 1.5 T while

performing a block-based visual task during 12 identical sessions of 216 s each. Both the acquisition and the reconstruction matrices were $64 \times 64 \times 35$ with the voxel size $3.8 \text{ mm} \times 3.8 \text{ mm} \times 3.75 \text{ mm}$. In all sessions, 72 volumes were acquired at $TR = 3 \text{ s}$, after discarding some 4 volumes to minimize the $T1$ saturation effects. A flashing checkerboard was presented in blocks of 24 s (On) followed by 24 s of fixation (Off), starting with rest (Figure 1).

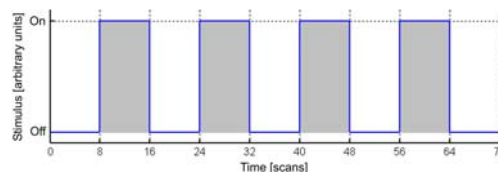


Figure 1. Experimental visual paradigm.

All data were subject to some preprocessing steps: (i) acquisition time correction, (ii) realignment (i.e., movement correction) and coregistration, and (iii) spatial normalization to the stereotaxic space. For analysis in both spatial domain (by SPM) and wavelet domain (by DWT), the same GLM was employed and designed in SPM2, which also included a model for the hemodynamic response function.

Data Analysis

Spectral domain

The human brain spontaneously generates neural oscillations with a large variability in frequency, amplitude, duration, and recurrence. Nevertheless, the long-term spatiotemporal structure of the complex patterns of the ongoing neural activity is less known, specifically, whether fluctuations in brain activity reflect a memory of the dynamics of the system in the range of a few seconds. It was found that the amplitude fluctuations of low frequency oscillations are correlated and obey power-law scaling behavior referred to as *long memory effect*. The large variability, the long-range correlations, and the power-law scaling behavior of spontaneous oscillations were consistently and unifying explained within the theory of self-organized *criticality*,

which provides a general mechanism for the emergence of correlations and complex dynamics in stochastic multiunit systems [24].

Wavelet methods are particularly adequate in brain imaging data analysis due to their broadly fractal properties exhibited by the brain in space and time. Besides, wavelet analysis is optimally decorrelating and performs Karhunen-Loève (KL) expansions [25] for long-memory processes. The temporal autocorrelation function is often transformed into the spectral domain, where the power-law decay for the correlations as a function of time translates into a power-law decay of the spectrum $S(f)$ as a function of frequency and led to terming it $1/f$ -like noise. Our results indicated the decay of the MR spectrum at low frequency following the $1/f$ dependence over at least 2 octaves (here from 10 Hz to 40 Hz) with a roll-off rate of about 12 dB/octave (Figure 2). In human beings, the $1/f$ noise is virtually omnipresent such as in heart beat rhythms, statistics of DNA sequences, and neural population activity.

Spatial domain

In SPM, a convolution with an isotropic symmetric Gaussian kernel is applied to preprocessed data prior to statistical analysis. Apart from its benefits, Gaussian filtering degrades the image resolution and complicates the subsequent statistical analysis since the noise can no longer be considered independent. The inferential methods test voxel-wise specific hypotheses about the expected changes in BOLD response. These changes are specified as regressors of interest in a (multiple) linear regression framework and their relative weights are given by the regression coefficients (i.e., model parameters). The voxel-wise test statistics form summary images known as statistical parametric maps, which are commonly assessed for statistical significance against the null hypothesis (e.g., no activation). The resulting map of a statistic is a representation of the spatial distribution of functional activity induced by the experimental task.

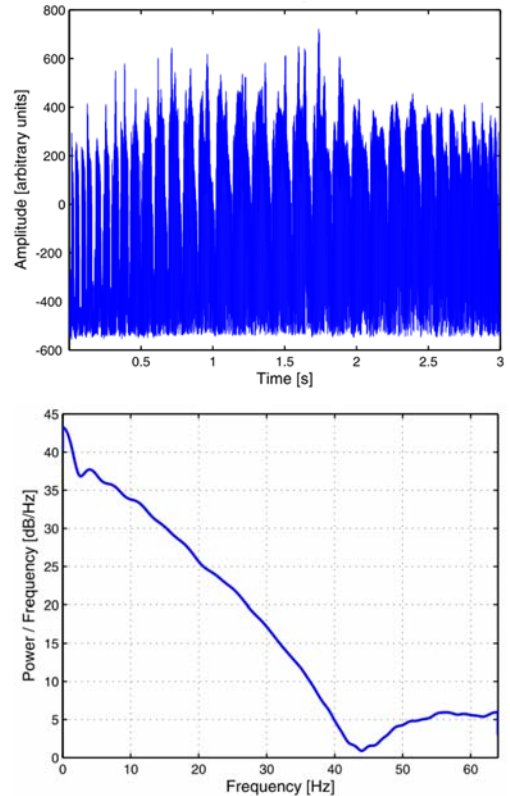


Figure 2. Preprocessed fMRI time series (top) have excessive power at low frequencies as indicated by the power spectral density (PSD) plot (bottom).

Denosing by Gaussian spatial filtering was successively carried out by means of in-plane smoothing kernels of 4×4 , 8×8 , 12×12 , and 16×16 mm \times mm, respectively (Figure 3.). The shape of the detected activation areas after denosing should not significantly deviate from that revealed by the raw time series. The active regions detected by SPM exhibited elliptic shapes with increasingly larger FWHM's of Gaussian kernels.

The denoised activation images were compared in all cases with the activation maps of the original raw data with minimum preprocessing in SPM (i.e., acquisition and movement corrections only) as a reference (Figure 4, left).

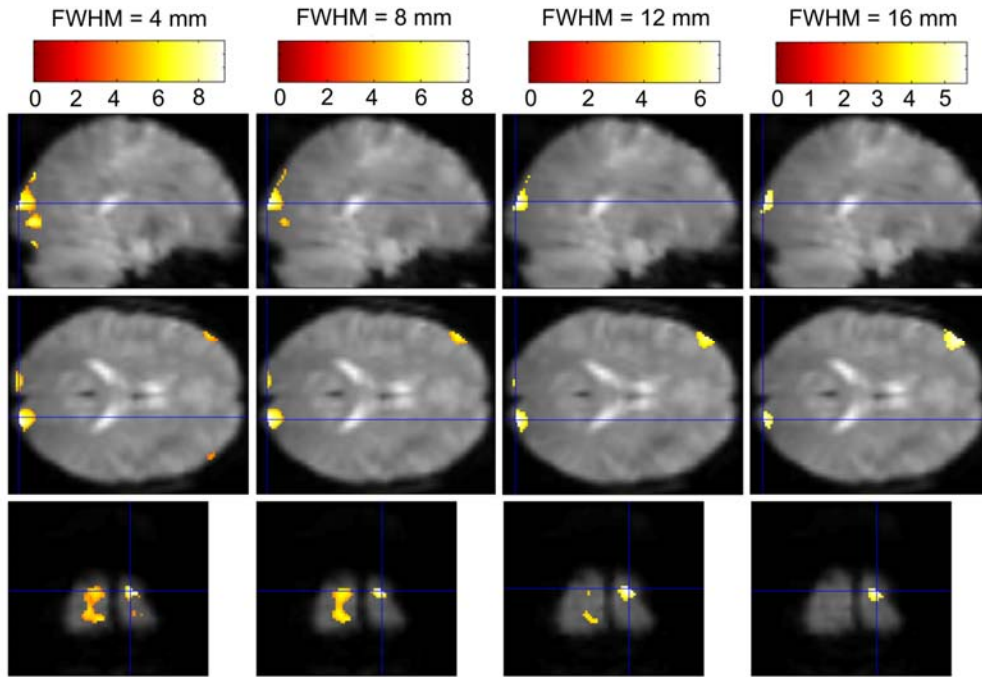


Figure 3. Spatial activation maps resulting from data smoothing with a Gaussian kernel of various sizes.

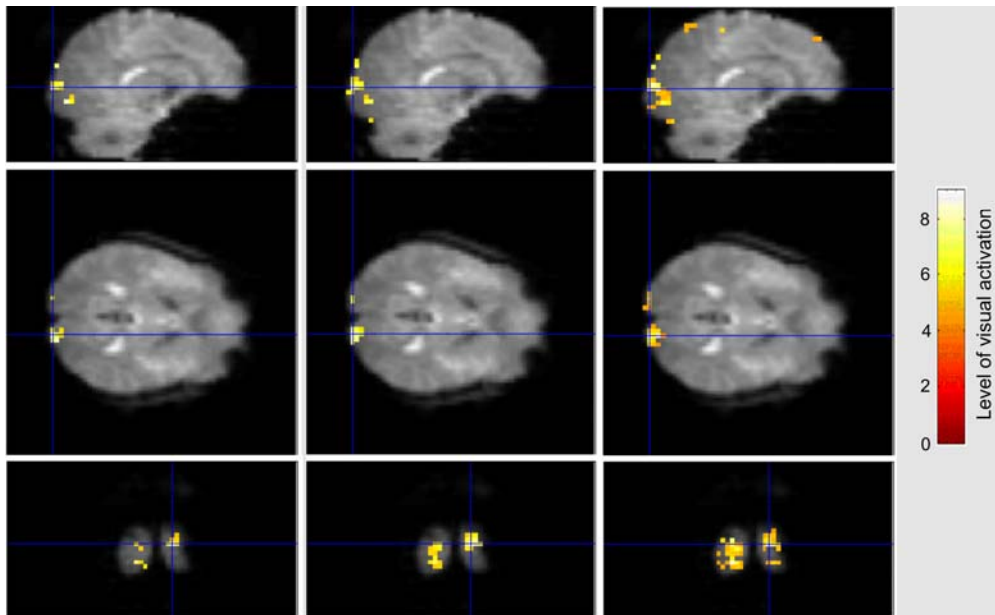


Figure 4. Brain activation parametric maps generated by: SPM with no spatial smoothing (left), SPM plus spatial Gaussian filtering (mid), and wavelet based statistical analysis (right).

Wavelet domain

The DWT was implemented by the separable 3D fractional-spline wavelets and 2D+Z quincunx wavelets [26]. Fractional splines are generalized cardinal splines depending on two parameters α and τ . The symmetric ($\tau=0$) fractional splines [27] were built using the FFT resulting the form of the *scaling function*:

$$\phi^\alpha(\omega) = \left| \frac{1 - \exp(-j\omega)}{j\omega} \right|^{\alpha+1}, j^2 = -1 \quad (10)$$

and the *two-scale relationship*:

$$\phi^\alpha(z) = \sqrt{2} \left| \frac{1+z^{-1}}{2} \right|^{\alpha+1} \quad (10)$$

in the spectral domain [2].

The same GLM used in SPM was applied to the time series of each wavelet coefficient. The activation pattern was spatially localized by the inverse DWT of the thresholded coefficient map and directly compared with the activation images obtained by statistical inference in the spatial domain (Figure 4, right). The corresponding time courses of activation resulting from SPM analysis (thresholding in the spatial domain) and wavelet-based analysis (shrinking in the wavelet domain) were highly correlated: $r > 0.9$ (Figure 4.). Less spatially variable t -statistic images and lower thresholds ($p < 0.05$) enforced better detection of activation and improved the physiological relevance of subsequent statistical inference.

The wavelet-based statistical analysis resulted in similar activation patterns as in SPM based on Gaussian random fields. Both approaches revealed bilateral activation within a network of visual responsive regions including the inferior occipital gyrus, fusiform gyrus, superior temporal sulcus, amygdala, inferior frontal gyrus, and orbitofrontal cortex (Figure 4). Since the shrinkage of the wavelet coefficients was carried out in the wavelet domain, the back-projected results were deployed of a direct statistical meaning in the signal domain (i.e., space or time domain). Yet the wavelet analysis came out with activation maps of higher resolution when the coefficients from the high-pass subbands were employed too.

For high SNR, both the large Gaussian spatial smoothing and the more smoothing wavelet-based denoising schemes introduced severe deformations and blurred the edges of the activated regions by introducing false negatives (type II errors). In contrast, for low SNR, the less smoothing methods, both Gaussian filtering and wavelets, generated false positives (type I errors). In the mid SNR range, the wavelet-based denoising methods led to less errors comparatively with Gaussian spatial filtering. However, only the smallest Gaussian smoothing kernel yielded realistic results (Figure 4). The wider smoothing kernels produced much larger detected areas (meaning more type I errors) or completely missed the active regions smaller than the kernel, in contrast to those obtained via less smoothing wavelet denoising methods.

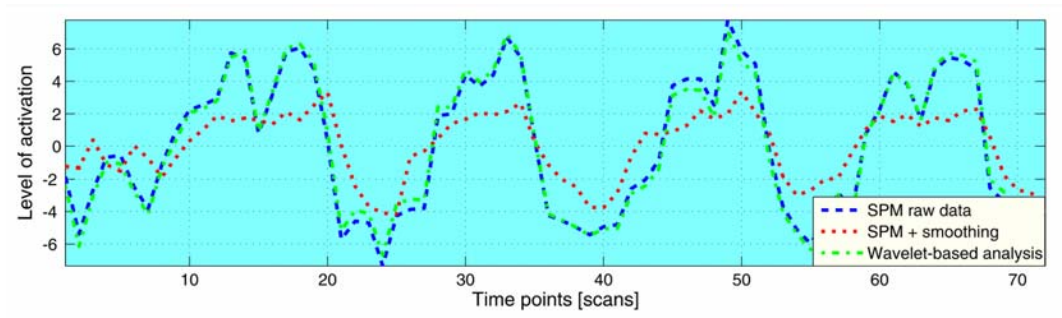


Figure 5. Associated time courses of activation of the maps showed in Figure 4.

Virtually for all wavelet-based methods, the output SNR is a linear function of the input SNR, that is, the wavelet methods, contrarily to Gaussian filtering, improve the SNR of the input images that already have a high SNR. It turns out that the wavelet-based denoising methods by introducing relatively little smoothness are generally preferably to Gaussian spatial smoothing for filtering fMRI time series.

4. CONCLUSIONS

Wavelet-based methods provide a naturally multiscale alternative to single scale Gaussian spatial smoothing and KL-like expansions for long-memory processes producing relatively decorrelated wavelet coefficients. Scale-varying wavelet-based methods for hypothesis testing of brain activation maps circumvent the need to specify a priori the size of signals expected and, therefore, the optimal choice of the smoothing kernel required by Gaussian filtering. Due to the smoothness of the wavelet representation, the estimated statistical parameter maps reveal more compact regions of activation than their counterparts obtained by statistic testing in spatial domain. The high frequency information contained in data is preserved in the wavelet subbands, contrarily to Gaussian filtering in SPM.

The preliminary findings so far pointed out that the methods producing smooth images introduce more false positives [22]. The less smoothing wavelet-based methods, though generating more false negatives, produce a smaller total number of errors than Gaussian filtering in spatial domain. As such, the wavelet-based denoising methods, by introducing less smoothing, preserve the sharpness of images and retain the original shapes of the active regions introducing less deformation. Likewise, wavelet analysis is optimal in terms of detecting transient events in fMRI time series and adapts well to local or nonstationary features in data within the scales of decomposition.

REFERENCES

- [1] K. J. Friston, A. P. Holmes, K. J. Worsley, J.-B. Poline, C. D. Frith, and R. S. J. Frackowiak, "Statistical Parametric Maps in Functional Imaging: A General Linear Approach," *Hum. Brain. Map.*, Vol. 2, pp. 189-210, 1995.
- [2] D. Van De Ville, T. Blu, and M. Unser, "Integrated Wavelet Processing and Spatial Statistical Testing of fMRI Data," *NeuroImage*, Vol. 23, No. 4, pp. 1472- 1485, 2004.
- [3] S. Ogawa, T. M. Lee, A. S. Nayak, and P. Glynn, "Oxygenation-Sensitive Contrast in Magnetic Resonance Image of Rodent Brain at High Magnetic Fields," *Magn. Reson. Med.*, Vol. 14, pp. 68-78, 1990.
- [4] U. E. Ruttimann, M. Unser, R. Rawlings, D. Rio, N. Ramsey, V. Mattay, D. Hommer, J. Frank, and D. Weinberger, "Statistical Analysis of fMRI Data in the Wavelet Domain," *IEEE Trans. Med. Imaging*, Vol. 17, No. 2, pp. 142-154, 1998.
- [5] K. J. Worsley, "Discussion of the Paper by Lange and Zeger," *Appl. Statist.*, Vol. 46, p. 25, 1997.
- [6] D. L. Donoho, "Nonlinear Wavelet Methods for Recovery of Signals, Densities, and Spectra from Indirect and Noisy Data," *Proc. Symposia in Applied Mathematics*, Vol. 00, 1993.
- [7] A. Hyvärinen, P. O. Hoyer, and M. Inki, "Topographic Independent Component Analysis," *Neural Comput.*, Vol. 13, No. 7, pp. 1527-1558, 2001.
- [8] R. Mutihac, "Sparse Decomposition of Brain Imaging Data – Wavelet Transform and Independent Component Analysis," *Proc. of OHBM*, p. 2360, Florence, 2006.

- [9] R. Crandall, *Projects in Scientific Computation*, pp. 197-198 and 211-212, Springer-Verlag, New York, 1994.
- [10] N. Bourbaki, "Topological Vector Spaces." In: *Elements of Mathematics*, 2nd edition, Springer-Verlag, Berlin, 2003.
- [11] S. G. Mallat, "A Theory for Multi-resolution Signal Decomposition: The Wavelet Decomposition," *IEEE Trans. Patter. Anal. Mach. Intell.*, Vol. 11, pp. 674-693, 1989.
- [12] M. Unser, P. Thevenaz, C. Lee, and U. E. Ruttiman, "Registration and Statistical Analysis of PET Images Using the Wavelet Transform," *IEEE Eng. Med. Biol. Mag.*, Vol. 14, pp. 603-611, 1995.
- [13] U. E. Ruttimann, M. Unser, D. Rio, and R. R. Rawlings, "Use of the Wavelet Transform to Investigate Differences in Brain PET Images between Patients," *Proc. SPIE*, Vol. 2035, *Mathematical Methods in Medical Imaging II*, pp. 192-203, San Diego, CA, 1993.
- [14] D. L. Donoho, "Unconditional bases are optimal bases for data compression," *Appl. Comput. Harmonica Anal.*, Vol. 1, pp. 100-115, 1993.
- [15] A. Cohen, I. Daubechies, and J. C. Feauveau, "Biorthogonal bases of compactly supported wavelets," *Commun. Pure Appl. Math.*, Vol. 45, pp. 485-560, 1992.
- [16] E. Bullmore, J. Fadili, M. Breakspear, R. Salvador, J. Suckling, and M. Brammer, "Wavelets and Statistical Analysis of Functional Magnetic Resonance Images of the Human Brain," *Statistical Methods in Medical Research*, Vol. 12, No. 5, pp. 375-399, 2003.
- [17] D. I. Hoult and P. C. Lauterbur, "The Sensitivity of the Zeugmatographic Experiment Involving Human Samples," *J. Magn. Reson.*, Vol. 34, pp. 425-433, 1979.
- [18] H. Gudbjartsson and S. Patz, "The Rician Distribution of Noisy MRI Data," *Magn. Reson. Med.*, Vol. 34, pp. 910-914, 1995.
- [19] W. A. Edelstein, P. A. Bottomley, and P. M. Pfeifer, "A Signal-to-Noise Calibration Procedure for NMR Imaging Systems," *Med. Phys.*, Vol. 11, pp. 180-185, 1983.
- [20] J. Sijbers, A. J. den Dekker, J. Van Audekerke, M. Verhoye, and D. Van Dyck, "Estimation of the Noise in Magnitude in MR Images," *Magn. Reson. Imag.*, Vol. 16, pp. 87-90, 1998.
- [21] R. D. Nowak, "Wavelet-Based Rician Noise Removal for Magnetic Resonance Imaging," *IEEE Trans. Image Processing*, Vol. 8, No. 10, pp. 1408-1419, 1999.
- [22] A. M. Wink and J. B. T. M. Roerdink, "Denoising functional Images: A Comparison of Wavelet Denoising and Gaussian Smoothing," *IEEE Trans. Med. Imaging*, Vol. 23, No. 3, pp. 374-387, 2004.
- [23] D. L. Donoho and I. M. Johnstone, "Adapting to Unknown Smoothness via Wavelet Shrinkage," *J. Am. Stat. Assoc.*, Vol. 90, No. 432, pp. 1200-1224, 1995.
- [24] K. L. Hansen, V. V. Nikouline, J. M. Palva, and R. J. Ilmoniemi, "Long-Range Temporal Correlations and Scaling Behavior in Human Brain Oscillations," *J. Neurosci.*, Vol. 21, No. 4, pp. 1370-1377, 2001.
- [25] M. Unser, "Splines: A Perfect Fit for Signal and Image Processing," *IEEE Signal Processing Mag.*, Vol. 16, pp. 22-38, 1999.
- [26] D. Van De Ville, T. Blu, and M. Unser, "Surfing the Brain: An Overview of Wavelet-Based Techniques for fMRI

Data Analysis,” IEEE Engineering in Medicine and Biology Magazine, Vol. 25, No. 2, pp 65-78, 2006.

- [27] M. Unser and T. Blu, “Fractional Splines and Wavelets,” SIAM Rev., Vol. 42, pp. 43-67, 2000.

AUTHOR INFORMATION



Radu Mutihac is professor in the Department of Electricity & Biophysics, University of Bucharest. His research interest is mostly focused on medical imaging (fMRI, EEG/MEG, digital mammography), image restoration and enhancement based on Bayesian inference with entropic prior, compartmental modeling and computer simulation of various nervous cells and simple neural networks, exploratory multivariate data analysis and data mining methods (ICA, FCA), wavelets, CAD techniques in VLSI analog and digital integrated circuits using advanced hardware description languages (VHDL, PSpice). During his academic career he joined as professor/research associate ICTP-UNU Microprocessor Laboratory, KU Leuven, Yale University, and Johns Hopkins University.